

On the growth dynamics of neutral vanadium oxide and titanium oxide clusters

M. Foltin, G. J. Stueber, and E. R. Bernstein

Citation: *The Journal of Chemical Physics* **111**, 9577 (1999); doi: 10.1063/1.480290

View online: <http://dx.doi.org/10.1063/1.480290>

View Table of Contents: <http://aip.scitation.org/toc/jcp/111/21>

Published by the [American Institute of Physics](#)

COMPLETELY

REDESIGNED!



**PHYSICS
TODAY**

Physics Today Buyer's Guide
Search with a purpose.

On the growth dynamics of neutral vanadium oxide and titanium oxide clusters

M. Foltin, G. J. Stueber, and E. R. Bernstein^{a)}

Department of Chemistry, Colorado State University, Fort Collins, Colorado 80523-1872

(Received 28 April 1999; accepted 3 September 1999)

Cluster growth dynamics of vanadium oxide and titanium oxide clusters produced by laser ablation of vanadium and titanium metal in a He gas flow seeded with up to 2% O₂ are studied by covariance mapping time-of-flight mass spectrometry. Covariance mapping enables the recognition of two different distribution components in the overall homogeneous mass spectra for both vanadium oxide and titanium oxide cluster systems. The oxygen-rich component Or shows small correlated fluctuations while the oxygen-poor component Op shows large correlated fluctuations. These two cluster distribution components are observed at low ablation laser powers and low expansion gas concentrations. Fluctuations of small vanadium oxide clusters (V₂O, V₂O₂, and V₂O₃) and small titanium oxide clusters (Ti₂O₂ and Ti₂O₃) are covariance determining. The less fluctuating V₂O₃ and Ti₂O₃ clusters are “nuclei” for the oxygen-rich components Or. The more fluctuating V₂O and Ti₂O₂ are “nuclei” for the oxygen poor components Op. Correlated fluctuations or covariances within each distribution component are constant. Covariances for the different distribution components are different. Studies of mass spectra and covariances as functions of ablation laser power and expansion gas concentration imply that V₂O and Ti₂O₂ clusters are formed in different regions of the ablation plasma plume than V₂O₃ and Ti₂O₃. We suggest that V₂O₃ and Ti₂O₃ are formed in the hot and optically dense region near the ablated metal surface and that V₂O and Ti₂O₂ are formed in the colder plasma region farther away from the ablated metal surface. Larger vanadium oxide and titanium oxide clusters grow from these small clusters by very specific pathways which involve only uptake of VO or VO₂, and TiO₂, respectively. © 1999 American Institute of Physics. [S0021-9606(99)00345-1]

I. INTRODUCTION

Early transition metal oxides are used as supports for metal catalysts and in many cases are found to be active catalysts themselves. For example, the Monsanto process uses a vanadium oxide catalyst for catalytic oxidation of SO₂ to SO₃ which is an important step in production of sulfuric acid.¹ Titanium oxide catalyst has been found to photo-oxidize CO, C₃F₆, and CH₃Cl to different sets of products depending on oxide surface structure.² Surface Ti³⁺ states can reduce D₂O to D₂ and NO to N₂O, respectively.² The nature of active sites on metal oxide surfaces is not well known. Surfaces of finely divided metal oxide powders have complicated morphologies consisting of various crystallographic planes, grain structures, and grain interfaces. Clusters of metal oxides formed in the gas phase, on the other hand, have relatively well-defined structures that vary systematically with cluster size. Some cluster geometries can mimic particular defect structures (e.g., kinks, islands, terraces) on metal oxide surfaces. Studies of reactivity of small metal oxide clusters as a function of cluster size can therefore aid in understanding the nature of low-coordinate reactive sites of metal oxide solids on a molecular level and under well-defined conditions. Gas phase clusters can thus represent a good model system for condensed phase properties and behavior.

Clusters of refractory metal oxides are typically produced by laser ablation of metal or metal oxide samples into a carrier gas (He, Ar) flow with added small amounts of oxidizer gas (1%–10% of O₂ or N₂O). The ablation plume, cooled by the carrier gas, reaches a high degree of supersaturation, so that cluster growth begins. Little is known about the dynamics of cluster growth in laser ablation plumes. Different cluster stoichiometries (i.e., metal/oxygen ratios) are typically obtained under various ablation conditions. Laser ionization mass spectrometry is employed to characterize neutral cluster distributions. Unfortunately, the stoichiometry of cluster ions may differ from the stoichiometry of their neutral precursors because of possible cluster fragmentation resulting from multiple photon absorption accompanying the ionization process.

In their pioneering work, Riley and co-workers³ were among the first to study mass spectral distributions of several transition metal oxide clusters including vanadium oxide, V_xO_y. In their experiment, vanadium metal is ablated at relatively low carrier gas pressure (~30–40 Torr) at the upstream end of a 6-cm-long channel; the ensuing metal clusters V_n are oxidized by 10% O₂ introduced in the carrier gas midway down the channel. The neutral cluster oxides are ionized by a second laser prior to their mass selection. Under these conditions, the average oxygen/metal ratio of V_xO_y⁺ cluster ions observed in the mass spectrum is $y/x \approx 1.4$ – 1.5 for $x \geq 4$. The 1–~1.5 V:O cluster stoichiometry appears to

^{a)}Electronic mail: erb@lamar.colostate.edu

correspond to high temperature, congruently vaporizing species in the vanadium oxygen phase diagram. This high temperature phase may result from exothermicity of the oxidation reaction of ablated V_n clusters with O_2 or from the multiphoton ionization process that deposits large amounts of energy in the cluster ion and can cause extensive cluster ion fragmentation.³ Under 1–10 J/cm² ionization laser fluence, clusters are first heated by absorption of 20 or more photons and subsequently ionized by thermionic emission accompanied by extensive fragmentation.

Different cluster stoichiometries have been reported for $V_xO_y^+$ cluster ions generated by laser ablation that are mass selected without postionization (and subsequent cluster ion fragmentation). Castleman and co-workers⁴ studied mass spectral intensities and reactivities of $V_xO_y^+$ cluster ions produced by laser ablation of vanadium metal into a pulsed flow of ~10% O_2 seeded in helium. In pulsed flow experiments, the carrier gas pressure at the ablation spot is estimated to be typically a few hundred Torr,⁵ i.e., about order of magnitude higher than in the work reported in Ref. 3. Under these conditions, cluster ions with stoichiometries $(VO_2)_n(V_2O_5)_m \times (O_2)_{0,2}^+$ are dominant in the cluster distribution.⁴ Collision-induced dissociation studies indicate that the additional O_2 units are only weakly attached to the stable clusters composed of VO_2 and V_2O_5 units.⁴ The 1:2–2:5 V:O ratios are consistent with the stoichiometry of bulk vanadium oxide.

In the present work we study the growth dynamics of vanadium oxide and titanium oxide clusters using the covariance mapping technique. Neutral clusters formed by laser ablation of vanadium or titanium metal, or of a pressed metal oxide powder, into a pulsed O_2/He flow are ionized by a second laser prior to their mass selection. The ~1–250 mJ/cm² ionization laser fluence employed in this study seems to be low enough for gentle (probably one or two photon) ionization of V_xO_y and Ti_pO_q neutral clusters with very little fragmentation (*vide infra*). The resulting mass spectra are very similar to those of Ref. 3, but, as revealed by covariance mapping studies, the cluster growth mechanism is different. This is not surprising since in our experiment the O_2 is mixed with the carrier gas upstream rather than downstream from the ablation spot. Interestingly, the neutral cluster stoichiometries do not reach the high oxygen/metal ratios observed for ionic clusters.⁴

Application of the covariance mapping technique to gain information supplemental to that obtained from conventional mass spectrometry is new in the metal oxide cluster field. Covariance mapping allows us to uncover correlations between different cluster peaks. If the simultaneous appearance (and also the simultaneous absence) of some peaks persists in most of the scans, these peaks are correlated. Normally, these correlations are lost by averaging the mass spectrum over several hundred to several thousand laser pulses to achieve reasonable signal to noise ratios. We record and store each single mass spectral scan i and calculate covariances $C(x,y)$ between any two mass spectral peaks x and y from a set of up to $n=2500$ scans in the usual way,

$$C(x,y) = \frac{1}{n} \sum_{i=1}^n (x_i - \bar{x})(y_i - \bar{y}) \quad (1)$$

in which

$$\bar{x} = \frac{1}{n} \sum_{i=1}^n x_i, \quad \bar{y} = \frac{1}{n} \sum_{i=1}^n y_i,$$

and x_i, y_i are signal intensities (integrated over peak areas) of mass spectral peaks x and y in mass spectral scan i . The covariance $C(x,y)$ is the measure of correlation between peaks x and y .

The mass peaks x and y may be correlated because of neutral cluster growth or cluster ion fragmentation. In our previous work on covariance mapping of toluene/water, aniline/argon, and fluorostyrene/argon clusters,⁶ we analyze in detail how growth and fragmentation contributions effect the covariance map and how they can be separated. In Sec. III we will show that under experimental conditions used in this study, covariances between different vanadium oxide and titanium oxide cluster peaks are growth dominated. We have shown before⁵ that the proper normalization for a growth dominated covariance $C(x,y)$ is the normalized covariance $\bar{C}(x,y)$ defined as

$$\bar{C}(x,y) = \frac{C(x,y)}{\bar{x}\bar{y}}. \quad (2)$$

We use this normalized form of covariance throughout this report.

Analyzing covariance data allows us to monitor the simultaneous or exclusive appearance of different peaks in the mass spectrum and to distinguish different components in the uniform overall mass distribution. This information cannot be obtained from conventional mass spectrometry. We show that the oxygen-poor vanadium oxide and titanium oxide cluster intensities have strong correlated fluctuations whereas the oxygen-rich cluster intensities correlate much less. This observation and careful studies of signal intensities as a function of expansion gas concentration and ablation laser power lead to the conclusion that small cluster precursors for oxygen-poor clusters (V_2O and Ti_2O_2) are formed in different regions of the ablation laser plume than the small cluster precursors for oxygen-rich clusters (V_2O_3 and Ti_2O_3). The larger clusters grow from these small precursors by very specific cluster growth pathways that involve the uptake of VO and VO_2 units in the case of vanadium oxide clusters, and of TiO_2 units in the case of titanium oxide clusters.

II. EXPERIMENTAL PROCEDURES

Neutral vanadium oxide and titanium oxide clusters are produced in a conventional laser vaporization/supersonic expansion cluster source by laser ablation of vanadium and titanium metal, respectively, into helium carrier gas mixed with up to 2% of O_2 or N_2O (under our experimental conditions, the cluster signal disappears for larger O_2 or N_2O concentrations). The pulsed oxygen/helium flow from an R.M. Jordan Co. pulsed nozzle operating at backing pressure 100 psig is injected through 0.8-mm-diam nozzle orifice into a 2-mm-diam, ~6-cm-long flow channel in the laser ablation

source. The metal of interest is ablated at laser energies of $\sim 2\text{--}20$ mJ/pulse by a 532 nm wavelength laser beam (second harmonic of a Nd/YAG laser) directed perpendicularly to the carrier gas channel and focused by an $f=100$ cm lens on the surface of a rotating and translating drum wrapped with a metal (vanadium or titanium) foil. The metal foil surface is tangential to the ablation channel wall and the ablation spot is approximately 2.75 cm downstream from the nozzle orifice. About 3.25 cm downstream from the ablation spot, the clusters entrained in the carrier gas flow freely expand into vacuum, and are carried by the ensuing molecular beam through a 1.5 mm skimmer into the ion source of a Willey–McLaren type TOF (time-of-flight) mass spectrometer where they are ionized by an ArF (193 nm) excimer laser beam. Most of the covariance data are recorded with a focused ionization laser beam at laser fluences from 2.5 to 250 mJ/cm². Under potential multiphoton ionization conditions like those employed in this work, clusters may fragment upon ionization. To ascertain the degree of cluster fragmentation, we compare mass spectral distributions and cluster signal intensities obtained with focused ionization laser beams at various laser fluences and obtained with unfocused laser beams at laser fluences ~ 2.5 mJ/cm².

The laser fluence is determined by dividing the laser beam radiant energy measured with a Molectron J-25 pyroelectric probe with the laser beam area measured at the ionization spot (note that the excimer laser beam intensity profile is roughly rectangular). The laser beam radiant energy is varied between 0.5 and 2 mJ. For a tightly focused ionization laser beam, the laser beam area is $3\text{ mm}\times 250\text{ }\mu\text{m}=0.0075\text{ cm}^2$ (the size of the laser beam induced burn spot on a photographic paper measured under a microscope). For an unfocused ionization laser beam, the laser beam area is $1\text{ cm}\times 5\text{ mm}=0.5\text{ cm}^2$.

The cluster ions so produced are extracted perpendicularly to the molecular beam and enter a 1.8-m-long flight tube in which they are separated in arrival time according to their mass. At the end of the flight tube, the ions are detected by Galileo microchannel plate detector. Signals from the detector are fed to a Tektronix RTD 720A transient digitizer and are sampled at 4 ns/bin and transferred after A/D conversion to a Gateway G6-180 computer for covariance calculations employing formulas (1) and (2) (for more detail, see Ref. 6). The Tektronix RTD 720A digitizer has fast data throughput to the computer over a GP-IB bus, enabling transfer of about 32 000 time bins (i.e., a mass spectral trace 128 μs long) per 100 ms at 8 bit vertical resolution. Thus, single TOF mass spectrometry (70 fms) scans can be recorded at a laser repetition rate of 10 Hz. Time delays between valve opening, firing the ablation laser, and firing the ionization laser are generated by two Stanford Research Systems digital delay generators DG 535.

Laser ablation of the V₂O₅ sample is also studied and vanadium oxide clusters are observed upon admixing 0.3% N₂O or 0.15% O₂ in the helium carrier gas and expanding the ablated/reacted mixture. For appropriate N₂O or O₂ concentrations (for example, 2% N₂O in case of metal ablation and

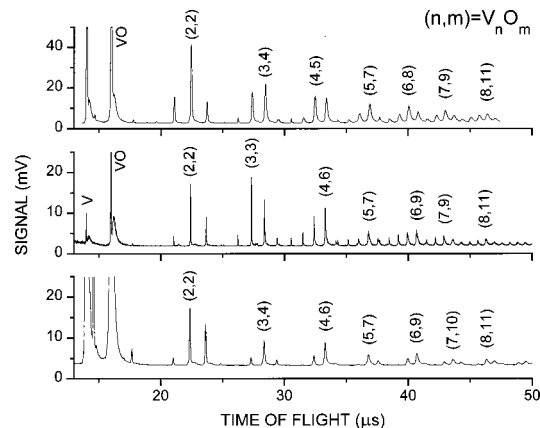


FIG. 1. Mass spectra of $V_n O_m$ clusters compared for different pulsed nozzle currents (related to different carrier gas concentrations in the ablation region) and O_x concentrations. The corresponding chamber pressures are 5×10^{-6} Torr (top trace), 9×10^{-6} Torr (middle trace), and 5×10^{-6} Torr (bottom trace). The O_x concentrations are $\sim 1\%$ O₂, $\sim 0.4\%$ O₂ (middle trace), and $\sim 2\%$ N₂O (bottom trace). Note that the number m of oxygen atoms in the most intense peaks $V_n O_m$, n constant, varies with the expansion conditions. This indicates that the $V_n O_m$ cluster distribution is controlled by cluster growth kinetics rather than by the thermodynamics or by cluster ion fragmentation (see the text).

0.25% N₂O in case of oxide ablation), cluster distributions generated by ablation of metal and metal oxide are almost identical.

To estimate cluster temperature in the molecular beam, mass resolved excitation spectra of the VO molecule are obtained by pumping the VO ($A\leftarrow X$) electronic transition with a tunable dye laser. The vibrational temperature of VO obtained by comparing intensities of the ($\nu'=1\leftarrow\nu''=0$) and ($\nu'=1\leftarrow\nu''=1$) vibronic transitions is about 950 ± 100 K. The cluster temperatures are expected to be lower: (1) although more oxidation reaction steps will occur for clusters than for VO, their number of internal degrees of freedom to share the excess energy is also proportionally higher; (2) their low frequency ‘‘phonon’’ modes will be cooled more efficiently in collisions with the expansion gas; and (3) larger clusters undergo an increased number of collisions with the carrier gas.

III. RESULTS

A. Vanadium oxide neutral cluster distribution

The $V_x O_y$ cluster size distribution, as observed in the mass spectrum (see Fig. 1), is comprised mostly of clusters of the general form $(VO)_n(VO_2)_m$. The distribution varies somewhat with cluster expansion conditions (i.e., the O₂ concentration, nozzle current, nozzle opening-ablation laser delay, etc.). In some spectra the V₃O₄, V₄O₆, V₆O₉, V₇O₁₀ features are most intense in the $V_x O_y$ (x constant, y variable) multiplets, whereas in other spectra the V₃O₃, V₄O₅, V₆O₈, and V₇O₉ features are most intense in their respective multiplets (see Fig. 1). This variation of peak intensity with cluster expansion conditions suggests that cluster growth is not completely controlled by thermodynamics and that growth kinetics also play an important role in the final cluster distribution.

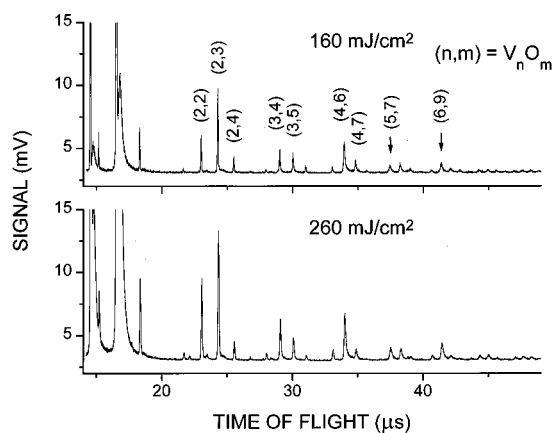


FIG. 2. Mass spectra of $V_n O_m$ clusters compared for different ionization laser fluences. The upper trace was recorded at 160 mJ/cm^2 . The lower trace was recorded at 260 mJ/cm^2 .

In general, under potential multiphoton ionization conditions such as those employed in this study, cluster ion fragmentation may be an issue. To ascertain the extent of cluster fragmentation, cluster size distributions and cluster signal intensities are observed as a function of the ionization laser fluence. The ionization laser fluence used in the present work is typically between 2.5 and 250 mJ/cm^2 . Decrease of ionization laser fluence by 37.5% reduces cluster ion signals by only about 35% (see Fig. 2). This implies a roughly linear dependence of cluster signal intensity on laser fluence (see the Appendix for a more thorough analysis of signal intensity variations with laser fluence). The distribution does not shift toward lower masses with increasing laser fluence. By adjusting the pulsed nozzle current and timing, we can produce somewhat more metal-rich cluster distributions than those shown in Fig. 1. As is well known from studies of the fragmentation behavior of vanadium oxide and other metal oxide cluster systems,⁷ the more metal-rich clusters are more prone to fragmentation because the vanadium metal-metal cluster bond is weaker than the metal-oxygen cluster bond (~ 60 vs $\sim 150 \text{ kcal/mol}$); however, even for these more metal-rich clusters we see no change in the cluster distribution upon decrease of the ionization laser fluence by almost two orders of magnitude (from 230 to 2.6 mJ/cm^2 —see Fig. 3). This fluence decrease is accomplished with an unfocused laser beam and leads to a signal intensity decrease of only a factor of 10. (In the Appendix we show that this signal intensity decrease upon defocusing the laser beam suggests that clusters are ionized by one- or two-photon ionization.)

Hackett and co-workers have performed two studies that support our conclusions of little or no cluster ion fragmentation at low ionization laser fluence ($\sim 2 \text{ mJ/cm}^2$) for $V_x O_y$ and $Ti_p O_q$ clusters. Reference 8 reports krypton photodesorption studies of $Nb_n Kr$, $5 \leq n \leq 15$, clusters in which Nb metal atoms are not desorbed from the cluster. The Nb-Nb bond energy is $\sim 120 \text{ kcal/mol}$ versus the V-O (and Ti-O) bond energy of 150 kcal/mol (and 160 kcal/mol). Reference 9 reports that for Ag_n , $2 \leq n \leq 16$, clusters coordinated to NH_3 , the relative abundance of Ag_n and $Ag_n NH_3$ can be inferred directly from intensities of their mass spectral peaks,

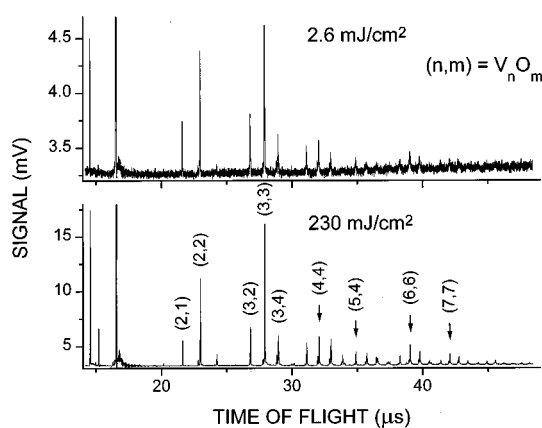


FIG. 3. Mass spectra of $V_n O_m$ clusters recorded with unfocused ionization laser beam (upper trace, laser fluence 2.6 mJ/cm^2) and with focused ionization laser beam (lower trace, laser fluence 230 mJ/cm^2).

and thus at $\sim 2 \text{ mJ/cm}^2$ laser fluence both Ag metal atoms and NH_3 adducts are not desorbed from the clusters (Ag-Ag bond strength is $\sim 40 \text{ kcal/mol}$). Riley and co-workers¹⁰ also make the point that for Ni_x , $x < 150$, and adsorbed NH_3 and H_2O (Ni-Ni bond energy $\sim 50 \text{ kcal/mol}$ and Ni- NH_3 and Ni- H_2O binding energies $< 20-40 \text{ kcal/mol}$) fragmentation is easily identified and can be eliminated by reduction of laser fluences, as we have done in these studies.

Thereby, under ionization laser fluences used throughout this work, the clusters are ionized by one- or two-photon ionization and cluster ion fragmentation is small. This conclusion is also supported by the following observation. We compare signal intensities at ionization wavelengths of 193 nm (generated by an ArF excimer laser) and 288 nm (generated by Nd-YAG pumped dye laser) at a laser fluence $\sim 250 \text{ mJ/cm}^2$. Cluster signal is observed only at 193 nm —no $V_x O_y$, $x > 1$, clusters are observed with an ionization laser wavelength of 288 nm . Absorption of two photons at 193 nm deposits about the same amount of energy in a $V_x O_y$ cluster as absorption of three photons at 288 nm . The absence of

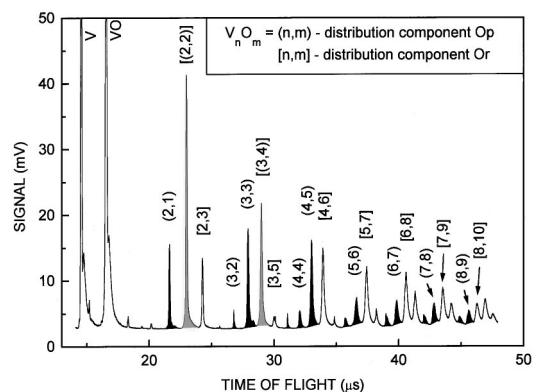


FIG. 4. The mass spectrum of $V_n O_m$ clusters. The mass peaks of the oxygen-poor distribution component Op are filled with black color and labeled (n,m) . The mass peaks of the oxygen-rich distribution component Or are unfilled and labeled $[n,m]$. The $V_2 O_2$ and $V_3 O_4$ mass peaks containing contributions from both distributions Op and Or are filled with gray color and labeled $[(n,m)]$. For the corresponding covariance matrix, see Table I. The corresponding cluster growth pathways are shown in Table II.

TABLE I. Normalized covariance matrix for V_nO_m clusters. (a) Covariances between cluster peaks from distribution component Op [i.e., $\bar{C}(x,y)$, $x \in \text{Op}$, $y \in \text{Op}$]. Note that most covariance values are between 0.047 and 0.066. Covariances involving V_2O_2 and V_3O_4 clusters (enclosed in parentheses) are smaller because V_2O_2 and V_3O_4 cluster intensities also have contributions from the distribution component Or. The errors in the covariances are presented as $\pm 2\sigma$. (b) Covariances between cluster peaks from distribution component Or [i.e., $\bar{C}(x,y)$, $x \in \text{Or}$, $y \in \text{Or}$]. Note that most covariance values are between 0.023 and 0.033. Covariances involving V_2O_2 and V_3O_4 clusters (enclosed in parentheses) are larger because V_2O_2 and V_3O_4 cluster intensities also have contributions from the distribution component Op. The errors in the covariances are presented as $\pm 2\sigma$. (c) Covariances between distribution components Op and Or [i.e., $\bar{C}(x,y)$, $x \in \text{Or}$, $y \in \text{Op}$]. Note that most covariance values are between 0.018 and 0.038. The errors in the covariances are presented as $\pm 2\sigma$.

(a)	$\bar{C}(\times 10^3)$	(V_2O_2)	V_3O_2	V_3O_3	(V_3O_4)	V_4O_4	V_4O_5	V_5O_6	V_6O_7	V_7O_8
	V_2O	(50 ± 12)	48 ± 8	60 ± 13	(44 ± 14)	66 ± 13	52 ± 15	60 ± 15	58 ± 15	54 ± 15
	(V_2O_2)		(31 ± 7)	(50 ± 14)	(44 ± 15)	(49 ± 12)	(46 ± 15)	(47 ± 14)	(44 ± 14)	(38 ± 13)
	V_3O_2			47 ± 8	(29 ± 8)	62 ± 9	38 ± 8	50 ± 9	51 ± 9	50 ± 10
	V_3O_3				(47 ± 15)	65 ± 14	53 ± 16	59 ± 16	57 ± 15	51 ± 15
	(V_3O_4)					(45 ± 14)	(45 ± 16)	(44 ± 15)	(42 ± 15)	(37 ± 14)
	V_4O_4						56 ± 15	67 ± 16	66 ± 16	63 ± 16
	V_4O_5							53 ± 17	52 ± 16	48 ± 16
	V_5O_6								61 ± 17	58 ± 17
	V_6O_7									60 ± 17

(b)	$\bar{C}(\times 10^3)$	V_2O_3	(V_3O_4)	V_3O_5	V_4O_6	V_5O_7	V_6O_8	V_6O_9	V_7O_9
	(V_2O_2)	(36 ± 13)	(44 ± 15)	(32 ± 12)	(36 ± 15)	(34 ± 14)	(32 ± 13)	(22 ± 13)	(28 ± 13)
	V_2O_3		(37 ± 13)	31 ± 11	35 ± 14	31 ± 12	26 ± 11	26 ± 11	22 ± 10
	(V_3O_4)			(33 ± 13)	(38 ± 16)	(35 ± 14)	(33 ± 14)	(26 ± 13)	(30 ± 13)
	V_3O_5				31 ± 13	28 ± 11	26 ± 10	23 ± 9	24 ± 10
	V_4O_6					33 ± 13	31 ± 12	29 ± 11	28 ± 12
	V_5O_7						31 ± 12	26 ± 10	29 ± 11
	V_6O_8							25 ± 10	30 ± 11
	V_6O_9								23 ± 9

(c)	$\bar{C}(\times 10^3)$	V_2O_3	V_3O_5	V_4O_6	V_5O_7	V_6O_8	V_6O_9	V_7O_9
	V_2O	30 ± 11	31 ± 11	31 ± 13	33 ± 13	34 ± 14	15 ± 12	31 ± 14
	V_3O_2	18 ± 6	28 ± 8	19 ± 9	22 ± 8	24 ± 8	8 ± 8	25 ± 8
	V_3O_3	35 ± 13	35 ± 12	36 ± 16	36 ± 14	35 ± 14	19 ± 13	33 ± 14
	V_4O_4	30 ± 11	36 ± 12	32 ± 14	34 ± 13	36 ± 14	15 ± 12	35 ± 14
	V_4O_5	34 ± 13	33 ± 12	37 ± 15	37 ± 15	36 ± 14	24 ± 13	34 ± 14
	V_5O_6	30 ± 11	33 ± 12	33 ± 15	36 ± 14	38 ± 15	19 ± 12	37 ± 14
	V_6O_7	26 ± 11	32 ± 11	32 ± 14	35 ± 14	38 ± 14	19 ± 12	38 ± 14
	V_7O_8	22 ± 10	28 ± 11	29 ± 13	32 ± 12	36 ± 13	18 ± 10	37 ± 13

cluster signal at 288 nm indicates that clusters are not ionized by very high order multiphoton absorption at laser fluences used throughout this work. Finally, covariance mapping also suggests that cluster ion fragmentation is weak. The covariance patterns discussed below are very different from those we have recently observed for highly fragmenting zirconium oxide clusters.¹¹

To learn more about the dynamics and kinetics of V_xO_y cluster growth, we perform covariance mapping studies under various expansion and laser ablation power conditions. Under most conditions, the normalized covariances $\bar{C}(V_xO_y, V_pO_r)$ are small and all constant, independent of the cluster size. These covariances are caused by neutral cluster growth rather than by cluster ion fragmentation. As previously discussed, under ionization conditions used throughout this work, the cluster fragmentation is weak. Under weak fragmentation conditions, clusters differing in size by one VO or VO_2 monomer unit would be expected to correlate more strongly than clusters differing by several monomer units. Thus, fragmentation controlled covariances would be expected to vary with cluster size. No such size

dependence of the covariance maps is observed. In our recent work on aniline/argon clusters⁶ we have shown that one possible explanation for size-independent normalized covariances is that the dominant fluctuation of cluster concentration occurs at an early stage in the neutral cluster growth. This may happen if an early step in the growth sequence is rate limiting (e.g., the aniline–Ar dimer formation⁶). In the V_xO_y case, the fluctuations of V_2O_2 or V_2O_3 concentration may account for size-independent normalized covariances (see the following discussion).

Under particular experimental conditions, mostly at low ablation laser power and with the ablation laser created plume close to the leading edge of the rising carrier gas pulse from the pulsed nozzle, the covariance map reveals that the observed V_xO_y mass distribution is composed of two different distribution components. The oxygen-rich clusters (i.e., V_2O_3 , V_3O_5 , V_4O_6 , V_5O_7 , V_6O_8 , V_7O_9 , and V_8O_{10} in Fig. 4) correlate weakly among themselves, as well as with the oxygen-poor clusters (see Table I). We denote the oxygen-rich distribution component Or. Conversely, the oxygen-poor clusters (i.e., V_2O , V_3O_2 , V_3O_3 , V_4O_4 , V_4O_5 , V_5O_6 , V_6O_7 ,

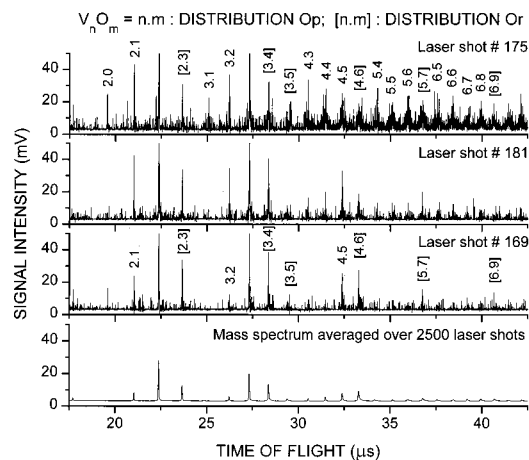


FIG. 5. Bottom trace: The mass spectrum of $V_n O_m$ clusters averaged over 2500 scans. Upper three traces: Three typical single scan mass spectra selected from the set of 2500 scans. Note that the signal intensities in oxygen-poor distribution Op (labeled n,m) vary greatly between the scans while the signal intensities in oxygen-rich distribution Or (labeled $[n,m]$) vary only very little.

$V_7 O_8$, and $V_8 O_9$ in Fig. 4) correlate strongly among themselves (see Table I). We denote the oxygen-poor distribution component Op. The fact that distribution components Or and Op correlate only weakly with each other indicates that they are formed independently, that is, one is not formed at the expense of the other [negative covariances would be expected in such a case, see Ref. 6 for fluorostyrene (Ar)_n].

Because large correlations in distribution component Op are observed only under special laser ablation/nozzle expansion conditions, the normalized covariance pattern discussed above is caused by cluster growth rather than by cluster ion fragmentation in the mass spectrometer. Moreover, fragmentation dominated normalized covariances would be expected to vary with cluster size, as previously pointed out. For example, $\bar{C}(V_6 O_7, V_5 O_6) = 0.061 \pm 0.017$ and $\bar{C}(V_6 O_7, V_2 O) = 0.058 \pm 0.015$ (see Table I) are the same within the (2σ) error bars. Furthermore, ion fragmentation of larger clusters usually feeds the most intense peaks in the mass spectrum. These belong to distribution component Or. Thus, strong correlation between distribution components Or and Op would be expected if the covariances were fragmentation dominated. Again, this is contrary to what is observed.

Cluster signal intensities in the oxygen-poor distribution component Op fluctuate more than in the oxygen-rich component Or and the covariance map shows that the strong fluctuations of different mass spectral peaks (cluster sizes) in component Op are correlated. Analysis of single laser pulse mass spectra shows that in many laser pulses the signal intensities in distribution component Op are close to zero while in some laser pulses they reach or even exceed signal intensities in distribution component Or (see Fig. 5). Conversely, the signal intensities in component Or vary little from one pulse to another and they do not seem to be affected by the observed bursts in component Op. This observation is consistent with low covariances between the two components or and Op of the total mass spectrum. The single pulse mass spectra emphasize that distribution Op is formed only under

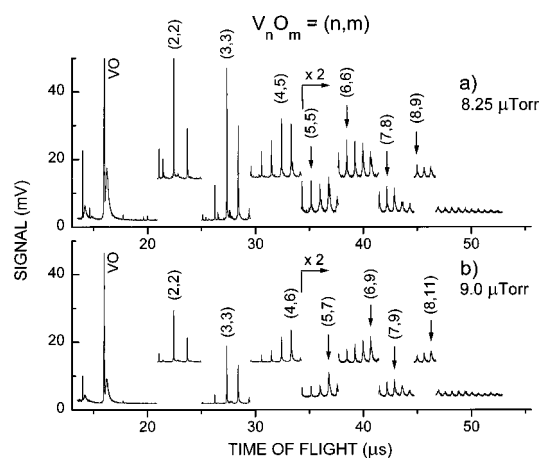


FIG. 6. Mass spectra of $V_n O_m$ clusters compared for different pulsed nozzle currents (related to different carrier gas concentrations in the ablation region). Upper panel: Lower nozzle current, resulting in chamber pressure 8.25×10^{-6} Torr. Lower panel: Higher nozzle current, resulting in chamber pressure 9.0×10^{-6} Torr. To help the viewer recognize peaks with constant number n of vanadium atoms and varying number m of oxygen atoms, the signal baseline is shifted for even numbers n . Note that the intensities of oxygen-poor clusters $V_4 O_5$, $V_5 O_{4-6}$, $V_6 O_{5-8}$, $V_7 O_{7-8}$, and $V_8 O_9$ drop significantly at higher valve current while the oxygen-rich cluster signal intensities $V_5 O_7$, $V_6 O_9$, $V_7 O_9$, and $V_8 O_{11}$ change only very little.

very special conditions and it occurs independently of, and concurrently with, distribution Or. The rather high signal intensities in distribution Op in the overall mass spectrum (i.e., averaged over 2500 laser pulses) arise because in some laser pulses the signal intensities in distribution Op are very high (see Fig. 5).

To get more insight into the formation mechanism of this special distribution component Op, mass spectra are studied as a function of pulsed nozzle current. Nozzle current determines effective nozzle opening area, the gas flow density from the nozzle, and consequently the gas concentration in the ablation region. Figure 6 shows that signal intensities for the oxygen-rich clusters (in particular, $V_4 O_6$, $V_5 O_7$, $V_6 O_9$, $V_7 O_9$, and $V_8 O_{11}$) vary only very little with nozzle current. Conversely, intensities of the oxygen-poor clusters (in particular $V_4 O_3$, $V_4 O_4$, $V_4 O_5$, $V_5 O_4$, $V_5 O_5$, $V_5 O_6$, $V_6 O_6$, $V_6 O_7$, $V_6 O_8$, $V_7 O_7$, $V_7 O_8$, and $V_8 O_9$) increase significantly upon lowering the nozzle current (lowering the gas concentration in the ablation region). This correlation between expansion gas concentration and cluster composition is consistent with the observation that the distribution component Op (the oxygen-poor component) becomes resolved from component Or in the covariance matrix under conditions for which the ablation laser plume intersects the leading edge of the rising carrier gas pulse from the pulsed nozzle. Thus, low gas concentration in the ablation region appears to support the formation of distribution Op.

Laser ablation of a vanadium oxide sample also generates vanadium oxide clusters in the helium carrier gas. For appropriate $N_2 O$ or O_2 concentrations (2% $N_2 O$ in case of metal ablation and 0.25% $N_2 O$ in case of oxide ablation), the cluster distributions generated by ablation of either metal or metal oxide are almost identical. Neutral metal oxide cluster formation mechanisms for ablation of either the metal or the

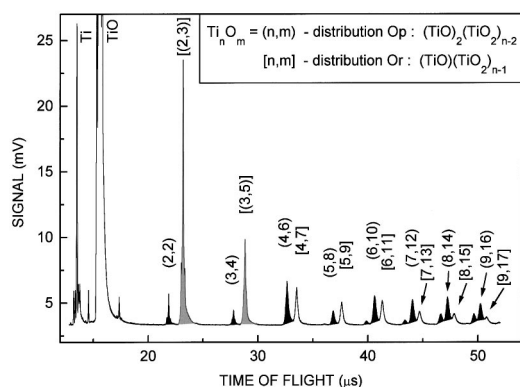


FIG. 7. The mass spectrum of $Ti_n O_m$ clusters. The mass peaks of the oxygen-poor distribution component Op are filled with black color and labeled (n,m) . The mass peaks of the oxygen-rich distribution component Or are unfilled and labeled $[n,m]$. The V_2O_3 and V_3O_5 mass peaks containing contributions from both distributions Op and Or are filled with gray color and labeled $[(n,m)]$. For the corresponding covariance matrix, see Table III. The corresponding cluster growth pathways are shown in Table IV.

metal oxide are thus very similar. A common feature for both metal and metal oxide ablation is high intensity of the VO peak in the mass spectrum, suggesting that VO may be an important building unit in the cluster growth. The signal fluctuations for vanadium oxide ablation are much higher than for vanadium metal ablation. The covariance matrix is dominated by large positive normalized covariance components that are independent of cluster size. These covariances are probably related to large fluctuations in the amount of ablated material from one pulse to another, caused by poor uniformity of the oxide sample. Better uniformity of the V_2O_5 sample will be necessary for covariance mapping studies of the cluster growth dynamics arising for V_2O_5 ablation.

B. Titanium oxide neutral cluster distribution

The mass spectra of titanium oxide clusters are dominated by $(TiO)(TiO_2)_n$ and $(TiO)_2(TiO_2)_{n-1}$ clusters (see Fig. 7). The covariance matrix of $Ti_p O_q$ clusters (Table II) shows very similar trends to those for the $V_x O_y$ clusters (Table I). Under special expansion conditions the cluster distribution is again composed of two distribution components Or and Op. The oxygen-rich component Or, comprised of the $(TiO)(TiO_2)_n$ series of clusters, shows small fluctuations and small normalized covariances. The oxygen-poor component Op, comprised of the $(TiO)_2(TiO_2)_{n-1}$ series of clusters, shows higher fluctuations and large normalized covariances. The covariances between components Or and Op are small. Observation of two different distribution components Or and Op for both the $V_x O_y$ and $Ti_p O_q$ clusters suggests that this bimodality of the overall cluster distribution is not caused by special chemistry for a particular system, but rather is related to a more general phenomenon occurring for metal oxide clusters formed by laser ablation of a metal sample followed by oxidation in an Ox/He gas flow (Ox = O_2 , N_2O , etc.). This phenomenon occurs under special experimental conditions; that is, for low expansion gas concentration and low ablation laser power.

IV. DISCUSSION

Two questions arise: (1) why under special beam and timing conditions does the independent second growth mode Op appear; and (2) what is the cluster formation mechanism? Two experimental conditions appear to facilitate the appearance of the component Op: low gas density in the ablation region and low ablation laser power. The following growth mechanism would be consistent with this finding and with observed cluster size independent normalized covariances for both the Or and Op distributions.

At low gas densities, metal vapor ablated from the surface can diffuse farther away from the surface where it becomes more dilute; thus, vapor concentration decreases with distance from the ablation spot. The plasma temperatures farther away from the surface will be lower, which will lead to smaller oxidation kinetic rates. Plausibly, at these larger distances some oxygen-poor small clusters will be formed (e.g., V_2O). Closer to the surface, the plasma temperature will be higher and oxidation kinetics will be faster. Plausibly, oxygen-rich small clusters will be formed close to the surface (e.g., V_2O_3). Larger clusters will grow from these small clusters by sequential uptake of VO or VO_2 or by the uptake of V followed by further oxidation. Constant (size independent) covariances in distributions Or and Op suggest that the dominant correlated fluctuation occurs in the formation of small clusters (V_2O_3 and V_2O). This fluctuation then propagates to larger cluster sizes as the clusters grow. Further uptake and/or oxidation of these “nuclei” occurs without much additional fluctuation (otherwise the normalized covariances would depend on cluster size). Since the oxygen-poor component Op fluctuates more than the oxygen-rich component Or (see Fig. 5), fluctuations of V_2O (formed farther from the surface) must be higher than fluctuations of V_2O_3 (formed closer to the surface). This can be explained by variations in the vapor concentration far from the surface.

Vapor concentration close to the surface may fluctuate less on a pulse to pulse basis because once high enough concentration is reached in this dense plasma region, the plasma becomes optically dense enough to absorb most of the laser light, thereby shielding the surface from further light absorption and ablation (see also Ref. 12). This shielding will have a stabilizing effect on the vapor concentration close to the surface, while the concentration away from the surface will fluctuate depending on the steepness of the temporal rise of the vapor density in the initial stage of the laser ablation pulse. At high ablation powers this increase in vapor density with time will be steep and only small amounts of vapor will reach the low density colder plasma region; thus the oxygen-poor distribution component Op occurs only at low ablation laser powers. At high carrier gas concentration in the ablation region, the vapor will not diffuse far enough from the surface and the clusters will be formed only in the hot region near the surface; thus, for these conditions, the distribution component Op is formed only when the ablation plume intersects the leading edge of the rising carrier gas pulse (i.e., in the low gas concentration region).

The above-mentioned mechanism also explains why at low gas concentrations the total number of clusters formed may be higher than at high concentrations and why those

TABLE II. Normalized covariance matrix of Ti_nO_m clusters. (a) Covariances between cluster peaks from distribution component Op [i.e., $\bar{C}(x,y)$, $x \in Op$, $y \in Op$]. Note that most covariance values are between 0.028 and 0.040. Covariances involving Ti_2O_3 and Ti_3O_5 clusters are enclosed in parentheses (the Ti_2O_3 and Ti_3O_5 cluster intensities also have contributions from the distribution component Or). (b) Covariances between cluster peaks from distribution component Or [i.e., $\bar{C}(x,y)$, $x \in Or$, $y \in Or$]. Note that most covariance values are between 0.016 and 0.020. Covariances involving Ti_2O_3 and Ti_3O_5 clusters (enclosed in parentheses) are larger because Ti_2O_3 and Ti_3O_5 cluster intensities also have contributions from the distribution component Op. (c) Covariances between distribution components Op and Or [i.e., $\bar{C}(x,y)$, $x \in Or$, $y \in Op$]. Note that most covariance values are between 0.020 and 0.028.

(a)	$\bar{C}(\times 10^3)$	(Ti_2O_3)	Ti_3O_4	(Ti_3O_5)	Ti_4O_6	Ti_5O_8	Ti_6O_{10}	Ti_7O_{12}	Ti_8O_{14}	Ti_9O_{16}
	Ti_2O_2	(39 ± 6)	36 ± 4	(29 ± 5)	40 ± 6	36 ± 5	36 ± 6	34 ± 6	32 ± 6	27 ± 6
	(Ti_2O_3)		(33 ± 5)	(33 ± 7)	(45 ± 9)	(34 ± 6)	(40 ± 8)	(37 ± 8)	(34 ± 8)	(31 ± 8)
	Ti_3O_4			(29 ± 4)	37 ± 5	34 ± 4	34 ± 5	33 ± 6	29 ± 5	27 ± 5
	Ti_3O_5				(37 ± 6)	(30 ± 5)	(33 ± 6)	(30 ± 6)	(28 ± 6)	(25 ± 6)
	Ti_4O_6					39 ± 6	46 ± 8	41 ± 8	39 ± 8	34 ± 8
	Ti_5O_8						36 ± 6	34 ± 6	31 ± 6	28 ± 6
	Ti_6O_{10}							39 ± 8	37 ± 8	34 ± 8
	Ti_7O_{12}								36 ± 9	33 ± 9
	Ti_8O_{14}									32 ± 9

(b)	$\bar{C}(\times 10^3)$	(Ti_3O_5)	Ti_4O_7	Ti_5O_9	Ti_6O_{11}	Ti_7O_{13}	Ti_8O_{15}	Ti_9O_{17}
	(Ti_2O_3)	(33 ± 7)	(28 ± 6)	(24 ± 6)	(23 ± 6)	(20 ± 5)	(18 ± 5)	(17 ± 5)
	(Ti_3O_5)		(26 ± 4)	(22 ± 4)	(21 ± 5)	(18 ± 4)	(16 ± 4)	(15 ± 4)
	Ti_4O_7			20 ± 4	21 ± 4	17 ± 4	16 ± 4	17 ± 3
	Ti_5O_9				18 ± 4	18 ± 3	16 ± 3	16 ± 3
	Ti_6O_{11}					17 ± 4	18 ± 4	18 ± 4
	Ti_7O_{13}						17 ± 4	18 ± 3
	Ti_8O_{15}							17 ± 4

(c)	$\bar{C}(\times 10^3)$	Ti_4O_7	Ti_5O_9	Ti_6O_{11}	Ti_7O_{13}	Ti_8O_{15}	Ti_9O_{17}
	Ti_2O_2	25 ± 5	24 ± 5	20 ± 5	21 ± 5	20 ± 5	18 ± 4
	Ti_3O_4	26 ± 4	24 ± 4	21 ± 4	23 ± 4	18 ± 4	22 ± 4
	Ti_4O_6	34 ± 6	28 ± 5	27 ± 7	23 ± 5	22 ± 6	21 ± 6
	Ti_5O_8	26 ± 4	25 ± 4	23 ± 5	23 ± 4	20 ± 4	20 ± 4
	Ti_6O_{10}	30 ± 5	26 ± 5	26 ± 6	23 ± 5	23 ± 6	22 ± 6
	Ti_7O_{12}	28 ± 6	25 ± 5	25 ± 6	25 ± 6	22 ± 6	22 ± 6
	Ti_8O_{14}	26 ± 6	24 ± 5	25 ± 7	23 ± 6	24 ± 7	21 ± 6
	Ti_9O_{16}	24 ± 5	21 ± 5	23 ± 7	22 ± 5	21 ± 6	23 ± 6

additional clusters at low concentrations are oxygen poor (see Fig. 6): the vapor concentration farther from the surface is higher at low gas pressures, whereas the vapor concentration close to the surface is determined primarily by the plasma optical absorption coefficient, and further vapor concentration buildup close to the surface is stopped as soon as the plasma becomes optically dense enough to absorb all incoming laser light.

Recall that the cluster size independent normalized covariances in distributions Op and Or suggest that large clusters grow from small cluster “nuclei.” Fluctuations in concentrations of these small clusters propagate in the cluster growth process to larger cluster sizes and determine covariances for the entire distribution. The distribution Op grows mainly from V_2O and the distribution Or grows mainly from V_2O_3 . Some clusters in both distributions will grow also from V_2O_2 . The V_2O_2 signal intensity fluctuates more than that of V_2O_3 but less than that of V_2O . The V_2O_2 signal intensity is most likely composed of low fluctuating and high fluctuating components. Apparently, some of the V_2O_2 is formed in the hot plasma region (the low fluctuating component) and some of it in the cold plasma region (the high fluctuating component).

Overlap between distributions Or and Op is small even

for large clusters, as evidenced by small normalized covariances between clusters from distributions Or and Op. This suggests that the cluster growth pathway for generating both distributions is very specific under given experimental conditions, as it involves the uptake of only VO or VO_2 (see Table III). The most intense peak in the mass spectrum is due to VO and larger clusters can be expected to grow by the sequential uptake of VO monomers. The VO_2 feature is weak in the mass spectrum, and perhaps the uptake of VO_2 may be a two-step process involving the uptake of VO and further oxidation.

In case of Ti_pO_q clusters the cluster growth pathway seems to be even more specific. The oxygen-rich distribution component Or comprising the cluster series $(TiO)(TiO_2)_n$ and the oxygen-poor distribution component Op comprising the cluster series $(TiO)_2(TiO_2)_{n-1}$ both grow by uptake of TiO_2 (see Table IV). Again, TiO_2 is weak in the mass spectrum and uptake of TiO_2 may be a two-step process involving uptake of TiO (the strongest peak in the mass spectrum) followed by further oxidation. Ti_2O_2 is the “nucleus” for the oxygen-poor cluster distribution Op. The Ti_2O_3 signal intensity has contributions from two components—the more fluctuating component is the second “nucleus” for the oxygen-poor cluster distribution Op, while the less fluctuating

TABLE III. Clusters observed in the mass spectrum and cluster growth pathways of vanadium-oxide clusters.

Low Ox concentration (~0.4% O ₂) (see also Fig. 5)		Medium Ox concentration (~1% O ₂) (see also Fig. 4)		High Ox concentration (~2% N ₂ O)	
Distribution Op	Distribution Or	Distribution Op	Distribution Or	Distribution Op	Distribution Or
V ₂ , V ₂ O, V ₂ O ₂	V ₂ O ₂ , V ₂ O ₃	V ₂ O, V ₂ O ₂	V ₂ O ₂ , V ₂ O ₃	V ₂ O, V ₂ O ₂	V ₂ O ₂ , V ₂ O ₃
↓ + VO	↓ + VO, VO ₂	↓ + VO, VO ₂	↓ + VO ₂	↓ + VO ₂	↓ + VO ₂
V ₃ O, V ₃ O ₂ , V ₃ O ₃	V ₃ O ₃ , V ₃ O ₄ , V ₃ O ₅	V ₃ O ₂ , V ₃ O ₃ , V ₃ O ₄	V ₃ O ₄ , V ₃ O ₅	V ₃ O ₃ , V ₃ O ₄	V ₃ O ₄ , V ₃ O ₅
↓ + VO ₂	↓ + VO, VO ₂	↓ + VO, VO ₂	↓ + VO, VO ₂	↓ + VO, VO ₂	↓ + VO, VO ₂
V ₄ O ₃ , V ₄ O ₄ , V ₄ O ₅	V ₄ O ₆	V ₄ O ₄ , V ₄ O ₅	V ₄ O ₆	V ₄ O ₅	V ₄ O ₆
↓ + VO	↓ + VO	↓ + VO	↓ + VO	↓ + VO ₂	↓ + VO ₂
V ₅ O ₄ , V ₅ O ₅ , V ₅ O ₆	V ₅ O ₇	V ₅ O ₅ , V ₅ O ₆	V ₅ O ₇	V ₅ O ₇	V ₅ O ₈
↓ + VO, VO ₂	↓ + VO ₂	↓ + VO	↓ + VO, VO ₂	↓ + VO	↓ + VO
V ₆ O ₅ , V ₆ O ₆ , V ₆ O ₇ , V ₆ O ₈	V ₆ O ₉	V ₆ O ₆ , V ₆ O ₇	V ₆ O ₈ , V ₆ O ₉	V ₆ O ₈	V ₆ O ₉
		↓ + VO	↓ + VO	↓ + VO, VO ₂	↓ + VO, VO ₂
		V ₇ O ₈	V ₇ O ₉ , V ₇ O ₁₀	V ₇ O ₉ , V ₇ O ₁₀	V ₇ O ₁₀ , V ₇ O ₁₁

component is the ‘‘nucleus’’ for the oxygen-rich cluster distribution or (see Table IV).

V. CONCLUSIONS

Covariance maps of V_xO_y and Ti_pO_q clusters, produced by laser ablation of vanadium and titanium metal, respectively, in an Ox/He (Ox=O₂, N₂O, etc.) gas expansion and ionized by ArF laser radiation at 193 nm at ionization laser fluences from 2.5 to 250 mJ/cm², are dominated by neutral cluster growth rather than cluster ion fragmentation. Different normalized covariance values for oxygen-rich and oxygen-poor clusters suggest two different distribution components in the overall homogeneous mass spectrum. The oxygen-rich component Or shows small correlated fluctuations while the oxygen-poor component Op shows large correlated fluctuations. The two different distributions are observed at low ablation laser powers and low expansion gas concentrations. The normalized covariances within each distribution component are cluster size independent. Fluctuations of V₂O, V₂O₂, and V₂O₃ small clusters are covariance determining and propagate to larger cluster sizes as clusters grow. The less fluctuating V₂O₃ is the ‘‘nucleus’’ for the oxygen-rich component Or. The more fluctuating V₂O is the

‘‘nucleus’’ for the oxygen-poor component Op. V₂O and V₂O₃ clusters are suggested to form in two different regions of the ablation plasma plume. V₂O₃ is formed in the hot and optically dense region near the ablated metal surface. The metal vapor density in this region fluctuates little. V₂O is formed in the colder plasma region farther away from the ablated metal surface. The metal vapor density in this region undergoes significant fluctuations. The V₂O₂ signal is composed of low fluctuating and high fluctuating contributions. The low fluctuating V₂O₂ formed in the hot plasma region is the second ‘‘nucleus’’ for distribution Or. The high fluctuating V₂O₂ formed in the cold plasma region is the second ‘‘nucleus’’ for distribution Op. Larger clusters grow from these small clusters by a very specific pathway that involves only uptake of VO or VO₂. The overlap between distribution components Op and Or is small. In the case of Ti_pO_q clusters, the oxygen-rich distribution component Or comprising the neutral cluster series (TiO)(TiO₂)_n grows from the Ti₂O₃ ‘‘nucleus’’ by sequential uptake of TiO₂. The oxygen-poor distribution component Op comprising the neutral cluster series (TiO)₂(TiO₂)_{n-1} grows mostly from the Ti₂O₂ ‘‘nucleus’’ by sequential uptake of TiO₂. Uptake of VO₂ and TiO₂, respectively, may be a two-step process involving first an uptake of VO and TiO, respectively, which are the most intense species in the mass spectrum, followed by further oxidation.

TABLE IV. Clusters observed in the mass spectrum and cluster growth pathways of titanium-oxide clusters.

Distribution Op	Distribution Or
Ti ₂ O ₂ , Ti ₂ O ₃	Ti ₂ O ₃
↓ + TiO, TiO ₂	↓ + TiO ₂
Ti ₃ O ₄ , Ti ₃ O ₅	Ti ₃ O ₅
↓ + TiO, TiO ₂	↓ + TiO ₂
Ti ₄ O ₆	Ti ₄ O ₇
↓ + TiO ₂	↓ + TiO ₂
Ti ₅ O ₈	Ti ₅ O ₉
↓ + TiO ₂	↓ + TiO ₂
Ti ₆ O ₁₀	Ti ₆ O ₁₁
↓ + TiO ₂	↓ + TiO ₂
Ti ₇ O ₁₂	Ti ₇ O ₁₃
↓ + TiO ₂	↓ + TiO ₂
Ti ₈ O ₁₄	Ti ₈ O ₁₅
↓ + TiO ₂	↓ + TiO ₂
Ti ₉ O ₁₆	Ti ₉ O ₁₇

ACKNOWLEDGMENTS

This work has been supported in part by the USARO and USNSF.

APPENDIX

In a (potentially) multiphoton ionization process, the signal intensity I will depend on the density of photon flux Γ (related to laser fluence F by the expression Γ = F/hν, in which hν is the photon energy), the number n of absorbed photons needed for the ionization, the cross sections σ_j, 1 ≤ i ≤ n, for absorption of the ith laser photon, the lifetime τ_i, 1 ≤ i ≤ n - 1, of the ith intermediate (real or virtual) ex-

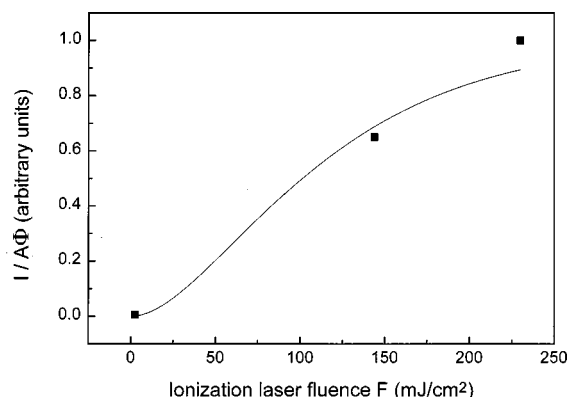


FIG. 8. Normalized cluster signal intensity ($I/A\Phi$) plotted as function of laser fluence. Solid squares: Experimental data points. Fitted curve: Obtained by fitting experimental data points with Eq. (A4). Note that all cluster sizes studied in this work show the same trend.

cited state involved in the multiphoton absorption, and the duration of the laser pulse, t . In the limiting case for which $\sigma_j\Gamma \ll 1$, the signal intensity I can be expressed as

$$I = NLA\Phi \left(\prod_{i=1}^{n-1} \sigma_i \frac{\tau_i}{t} \right) \sigma_n \Gamma^n. \quad (\text{A1})$$

In Eq. (A1) N is the concentration of clusters of given cluster size in the molecular beam, L is the length of the intersection of the laser beam with the molecular beam, A is the ionization laser beam cross section in the region where it intersects the molecular beam, and Φ is the collection efficiency of the mass spectrometer ($\Phi < 1$ if the laser beam height is larger than the molecular beam height or if the ion optics of the mass spectrometer do not allow ion extraction from the whole area illuminated by the laser beam). Note that if the lifetime $\tau_i > t$, the ratio τ_i/t in Eq. (A1) has to be replaced by the number 1. Hence, the signal intensity ratio I_1/I_2 for ionization by an unfocused laser beam (laser fluence F_1 , laser beam cross section A_1) and ionization by a focused laser beam (laser fluence F_2 , laser beam cross section A_2) can be expressed as

$$I_1/I_2 = (A_1/A_2)(\Phi_1/\Phi_2)(F_1/F_2)^n. \quad (\text{A2})$$

Since the laser beam cross section and laser fluences are known, the average number of absorbed photons n can be estimated from

$$n = \frac{\ln[(I_1/I_2)(A_2/A_1)(\Phi_2/\Phi_1)]}{\ln(F_1/F_2)}. \quad (\text{A3})$$

According to Fig. 3, the signal intensity decreases 10 times ($I_1/I_2 = 0.1$) if the laser beam fluence is reduced about 90 times ($F_1/F_2 = 0.011$) by defocusing the laser beam ($A_1/A_2 = 67$) at laser beam energies $Q_1 = 1.3$ mJ and $Q_2 = 1.75$ mJ. Substituting these numbers in Eq. (A3) yields $n = 1.45$. This number has to be corrected with regard to decrease in collection efficiency of the mass spectrometer for the defocused ionization laser beam, as ions are extracted into the mass spectrometer only from a part of the $1 \text{ cm} \times 5 \text{ mm}$ area illuminated by the defocused laser beam. Assuming $\Phi_1/\Phi_2 = 25\%$, one obtains $n = 1.15$. Thus, the number of photons needed for ionization is small.

Equation (A3) has been derived under the assumption that $\sigma_1\Gamma \ll 1$. If $\sigma_1\Gamma \sim 1$, some saturation in the dependence of signal intensity on laser fluence may occur. For two-photon ionization and under the simplifying assumptions that $\sigma_1 = \sigma_2 = \sigma$ and $\tau > t$, the signal I can be expressed as

$$I/(A\Phi) = NL \left(1 - e^{-\sigma(F/h\nu)} - \sigma \frac{F}{h\nu} e^{-\sigma(F/h\nu)} \right). \quad (\text{A4})$$

Figure 8 presents a fit of Eq. (A4) to the measured dependence of $I/(A\Phi)$ on laser fluence F using the cross section σ as a fitting parameter. Evidently, the measured signal intensities show less saturation with increasing laser fluence than that predicted by Eq. (A4).

¹I. A. Campbell, *Catalysis at Surfaces* (Chapman and Hall, New York, 1988).

²(a) J. Fan and J. T. Yates, *J. Phys. Chem.* **98**, 10621 (1994); (b) G. Lu, A. Linsebigler, and J. T. Yates, *ibid.* **98**, 11733 (1994); (c) J. C. S. Wong, A. Linsebigler, G. Lu, J. Fan, and J. T. Yates, *ibid.* **99**, 335 (1995); (d) G. Lu, A. Linsebigler, and J. T. Yates, *J. Chem. Phys.* **102**, 3005 (1995); (e) **102**, 4657 (1995).

³G. C. Nieman, E. K. Parks, S. C. Richtsmeier, K. Liu, L. G. Pobo, and S. J. Riley, *High. Temp. Sci.* **22**, 115 (1986).

⁴R. C. Bell, K. A. Zemski, K. P. Kerns, H. T. Deng, and A. W. Castleman, Jr., *J. Phys. Chem. A* **102**, 1733 (1998).

⁵S. Maruyama, L. R. Anderson, and R. E. Smalley, *Rev. Sci. Instrum.* **61**, 3686 (1990).

⁶M. Foltin, G. J. Stueber, and E. R. Bernstein, *J. Chem. Phys.* **109**, 4342 (1998).

⁷C. Brechignac, Ph. Cahuzac, F. Carlier, M. de Frutos, J. Leygnier, and J. Ph. Roux, *J. Chem. Phys.* **99**, 6848 (1993).

⁸B. A. Collins, K. Athanassenas, D. M. Rayner, and P. A. Hackett, *Z. Phys. D* **26**, 36 (1993).

⁹L. Lian, S. A. Mitchell, P. A. Hackett, and D. M. Rayner, *J. Chem. Phys.* **104**, 5338 (1996).

¹⁰E. K. Parks, B. J. Winter, T. D. Klots, and S. J. Riley, *J. Chem. Phys.* **94**, 1882 (1991).

¹¹M. Foltin, G. J. Stueber, and E. R. Bernstein, (unpublished).

¹²G. Dietz, M. A. Duncan, D. E. Powers, and R. E. Smalley, *J. Chem. Phys.* **74**, 6511 (1981); see also J. F. Ready, *Effects of High Power Laser Radiation* (Academic, New York, 1971).